Colloid Polym Sci (2008) 286:1545–1552
DOI 10.1007/s00396-008-1929-4

ORIGINAL CONTRIBUTION

The effect of fructose derived carbon shells on the plasmon resonance and stability of silver nanoparticles

John C. Heckel · Fatimah F. Farhan · George Chumanov

Received: 11 July 2008 / Revised: 4 September 2008 / Accepted: 4 September 2008 / Published online: 18 September 2008

Abstract Carbon nanoparticles between 10 and 50 nm in diameter and carbon shells of various thickness around silver nanoparticles were synthesized by the hydrothermal reaction of fructose. The effect of the carbon shells on the plasmon resonance of the silver nanoparticles and their stability in sodium chloride solutions was investigated. The shell thickness can be adjusted to have insignificant damping of the plasmon resonance and provide stabilization of the particles in solutions with high ionic strength. Hydrazine–carbonyl cross-linking reactions were performed to link fluorescent dye molecules to carbonyl groups on the carbon shell surface.

Keywords Core shell · Silver nanoparticle · Carbon nanoparticle · Hydrothermal · Fructose

Introduction

There is currently great interest in composite nanostructures consisting of two or more materials allowing the combination of different properties into one small entity. Silver nanoparticles (NPs) interact efficiently with light via the excitation of plasmon resonances which are the collective oscillations of the free electron density [1]. In fact, the excitation of plasmon resonances in Ag NPs represents the most efficient mechanism by which light interacts with matter [2]. Therefore, plasmonic Ag NPs are promising building blocks for various photonic applications [1] and are widely used for surface-enhanced Raman scattering (SERS) [3, 4] and enhanced fluorescence [5, 6] spectroscopy as well as biological imaging [7–10]. For many applications, Ag NPs require protective shells because they can easily aggregate in high ionic strength solutions or in solutions containing molecules that have affinity to the silver surface. In addition to the protection function, the shell should provide a scaffold for easy surface modification of NPs. Strategies for protecting and modifying Ag NP include encapsulation into dielectric shells such as silica and titania via the sol–gel chemistry [11, 12], polymers by emulsion polymerization [13], and adsorption of long aliphatic chains [14] or short peptides and amino acids [15] through the self-assembly technique. The shell should be nonmetallic; otherwise, quenching of the plasmon resonance can occur. Carbon is an alternative shell material because it is inert, robust, and has been reported to be a biocompatible layer on artificial implants [16]. Good sources of carbon are hydrothermally treated sugars and cellulose. This approach was used to synthesize carbon nano- and micron-sized particles and mesoporous structures [17–20].

The formation of carbon shells around magnetic nanoparticles [21, 22] as well as on Ag NPs and other Ag nanostructures by the hydrothermal reaction of glucose was previously reported by Yadong Li and others [18, 23–27]. The work presented here focuses on the effect of the carbon shell on the plasmon resonance of different-sized Ag NPs and on the stability of these nanoparticles (C:Ag NPs) in electrolyte solutions as well as on their surface modification. In addition, the hydrothermal reaction of fructose without Ag NPs in water was studied. This reaction resulted in the formation of carbon nanoparticles (C NPs) of significantly smaller size than previously reported. The analysis of this reaction helped to understand the formation

J. C. Heckel · F. F. Farhan · G. Chumanov (✉)
Department of Chemistry, H. L. Hunter Laboratory,
Clemson University,
Clemson, SC 29634, USA
e-mail: gchumak@clemson.edu

of the carbon shells around Ag NPs. Silver NPs were synthesized by the hydrogen reduction of silver oxide yielding aqueous suspensions of single crystal, monodispersed particles of different sizes that can be easily controlled [28]. Fructose was used as a carbon source for the shells and C NPs. The NPs were characterized by scanning electron microscopy (SEM), transmission electron microscopy (TEM), UV–vis extinction spectroscopy, and Raman spectroscopy.

Materials and methods

Silver (I) oxide (99.99% purity) received from Sigma Aldrich, NaCl received from Fisher, Alexa Fluor 488 received from Invitrogen, carbohydrazide received from Acros, and fructose purchased from a local grocery store were used without further purification. A glass pressure tube was purchased from Ace Glass. Slide-A-Lyzer dialysis cassettes (10 K MWCO) were purchased from Thermo Scientific. UV–vis extinction spectra were recorded with a Shimadzu 2501PC spectrophotometer. TEM images were obtained with a Hitachi 7650, and the SEM image was obtained with a Hitachi 4800 electron microscope. SERS and Raman spectra were recorded using Triax 550 spectrograph equipped with a CCD detector, model Symphony 1024×256-BIDD-1LS (Jobin Yvon), coupled to a microscope (Olympus IX71) with a 20× objective. Fluorescence spectra were recorded using a Photon Technology International flourometer.

C NPs were synthesized by dissolving 0.1–1 M fructose in 10 mL of milliQ (Millipore) DI water in a 20-mL glass pressure tubes and sealed with a Teflon cap and Viton o-ring. The pressure tube was placed in an aluminum heating block and sand was poured into the space between the aluminum block and the tube. The reaction temperature was monitored from a thermometer in the aluminum block which was placed on a hot plate. The fructose solutions were heated to 110 and 130 °C over 1 h and held at that temperature for 6–23 h. After cooling down to room temperature, the product was transferred into a dialysis cassette and dialyzed against milliQ water for purification of the C NPs. The C NPs were also treated at supercritical conditions. Fifty milliliters of C NPs synthesized from 0.4 M fructose for 7 h was purified and concentrated into 2-mL volume. The concentrated C NP solution was transferred into a 3/8″×4″ silver ampoule which was welded shut on both ends. The ampoule was then placed in a 27-mL Inconel autoclave and counter-pressured with water. The sample was heated at 400 °C for the duration of 1 week. No further purification of the sample was done before analysis. Ag NPs were synthesized by reduction of Ag_2O by H_2 gas in milliQ DI water according to the previously described procedure [28]. To form carbon shells, fructose was dissolved in 10 mL of aqueous Ag NP suspensions with optical density of approximately 1 to obtain final fructose concentrations of 0.1–0.4 M. The temperature was brought to 130 °C over the course of 1 h and held at this temperature for 5 h before being allowed to cool down to the room temperature. The product was centrifuged and washed with water and ethanol five to six times or until the supernatant showed no absorption in the UV spectral range.

The stability of C:Ag NP was tested by dispersing the NPs in 0.2 M NaCl and compared to that of unmodified Ag NPs. The solution was stirred for 24 h, and UV–vis extinction spectra were recorded prior and after the exposure to NaCl. To determine the relative size of pores in the carbon shell, SERS measurements of adenine were undertaken from C:Ag NPs. Saturated adenine solution (100 μL) was added to 2 mL of Ag NPs and 2 mL of C:Ag NPs synthesized with 0.25 M fructose and stirred for 4 h to allow adsorption of adenine. The NPs were centrifuged and dried onto a microscope slide and SERS spectra were recorded.

In order to experiment with C:Ag NPs surface modification, a hydrazine–carbonyl cross-linking reaction was performed. A 1 mL solution containing C:Ag NPs of optical density 2 was diluted to 1.5 mL using carbohydrazide dissolved in water to make the final carbohydrazide concentration 10 mM. A C:Ag NPs solution of the same volume and concentration was prepared with no carbohydrazide. A drop of concentrated HCl was added to both the solutions to begin the cross-linking reaction which was stirred for 2 h. After this time, a small volume of Alexa Fluor 488 was added to both solutions, making their concentration 2.5 μM, followed by stirring overnight. The solutions were centrifuged, and the C:Ag NPs were resuspended three times to wash away free Alexa. Fluorescence emission spectra were measured by exciting at 495 nm and recording between 505 and 600 nm.

Result and discussion

Prior to the deposition of the carbon shell around Ag NPs, the hydrothermal reaction of fructose without Ag NPs was carried out in water. Under hydrothermal conditions, fructose undergoes dehydration and hydrolysis reactions to form many products including hydroxymethylfurfural (HMF), 2-(2-hydroxyacetyl)furan (HAF), various acids, and carbonaceous precipitate [29–32]. Glucose behaves similarly forming carbonaceous precipitate as a result of the hydrothermal reaction. Fructose generally requires lower temperatures than glucose to form carbonaceous precipitate [17]. The carbonaceous precipitate forms colloidal particles

between 80 nm and 5 μm, as was previously reported [17–19]. The composition of particles depends on the temperature and duration of the reaction, whereas longer reaction time and/or higher temperature cause more carbonization. After complete loss of water from sugars, a graphitic phase is formed. The starting concentration of fructose is also important because it determines the concentration of C NPs. C NPs form at lower temperature (<200 °C) and/or during shorter reactions (<12 h), whereas longer reaction time (>12 h) and/or higher temperature (>200 °C) yield rather large aggregated precipitates. Higher reaction temperature and time also result in carbon precipitates containing more graphitic phase due to loss of more water from the sugars.

A possible mechanism for the formation of the carbonaceous precipitate was described in [18], according to which, the process starts with the dimerization of glucose molecules and continues with the formation of larger oligomers. After reaching a critical concentration, oligomers aggregate into NPs with minimum size of approximately 150 nm. However, Yao et al. [17] have shown C NPs of approximately 80-nm diameter synthesized from glucose. In our experiments, the hydrothermal reaction of fructose at 110 °C resulted in approximately 10 nm C NPs. It is believed that the formation of such small C NPs does not necessarily require the oligomerization but rather the condensation of small monomeric fructose dehydration products such as HAF and HMF molecules that act as initial seeds. It has also been shown that carbonaceous precipitate formed from the hydrothermal reaction of HMF alone [29]. The difference between this model and the mechanism described in [18] is that the growth of C NPs took place by stepwise condensation of molecules, similar to a sol–gel reaction, as opposed to the sudden aggregation of oligomers. Elevated heat and pressure caused the further carbonization of small NP seeds, and as more fructose molecules dehydrated and reacted with the seed, NPs grew further. The core of the NP was carbonized to a higher degree, while the surface just began the carbonization process. The less-carbonized surface contained the hydroxyl and carbonyl functional groups from HAF for example, as well as carboxyl groups from the oxidation of carbonyls during the reaction [17, 18, 24]. In addition, acid, which is formed during the reaction, self-catalyzed the carbonization of sugar [32]. If time and temperature permit, this process will lead to aggregation of the C NPs, as the particles grow too large to remain in colloidal suspension or all the fructose molecules have been depleted and the large C NPs aggregate and continue to carbonize becoming more graphitic.

To test this model, 0.1–0.6 M aqueous fructose solutions were heated for 7–24 h at 110 and 130 °C in pressure tubes. Purified C NPs synthesized from 0.4 M fructose were additionally treated in supercritical water at 400 °C for 1 week. Images of the products obtained at the two extreme conditions, specifically at 110 °C for 7 h and 400 °C for 1 week, are shown in Fig. 1a,f, respectively. Independent of fructose concentration, the 7-h reaction yielded what appeared to be a film with a few imbedded C NPs. Such structure was indicative of the beginning stage of C NP formation, for which the reaction time was not sufficient for the seeds to grow into larger NPs. The film most likely consisted of very small NPs because it was retained by a dialysis membrane with 10 kDa (about 1- to 4-nm pore size) cutoff. The supercritical treatment, on the other hand, resulted in complete aggregation of C NPs because the solution did not contain fructose molecules, and as the reaction proceeded, the surface of the C NPs continued to carbonize and finally lose all functional groups on the surface and, consequently, solubility in water. As the reaction time was increased to 12 h at 110°C, C NPs with the diameter between 10 and 40 nm were formed depending on fructose concentration (Fig. 1b–d). Smaller C NPs appeared to have more irregular shape and were more polydispersed compared with larger C NPs. This surface irregularity and polydispersity was due to loosely bound, not fully carbonized species that defined the size and shape of the small C NPs. As the size of the NPs increased, the core became more carbonized and the particles appeared more spherical and monodispersed (Fig. 1e). This trend is commensurate with the model for growth of C NPs based on the condensation of HMF and HAF molecules. Twenty-four-hour reaction times at low temperature formed large aggregates analogous in appearance to those shown in Fig. 1f. Reactions at higher temperatures resulted in larger C NPs for the same reactions time. For example, 7 h at 130 °C resulted in C NPs with diameters of about 50 nm (Fig. 1e). It is important to note that either the reaction time or the temperature can both be adjusted to result in the same size C NPs, so that shorter reactions at higher temperatures yield the same particles as longer reactions at lower temperatures. Particles as large as 1 μm were also synthesized using higher fructose concentrations (data not shown).

Raman spectroscopy was used to characterize C NPs (Fig. 2). Raman spectra of all samples are quite complex and can be characterized by the presence of two broad bands with several distinct shoulders the origin of which is currently unknown. The band at 1,345 cm^{-1} is called the D-band and is characteristic of a disordered carbon, and the band at 1,585 cm^{-1} is the G-band corresponding to the first-order phonon of graphite and is representative of a more graphitic structure [33]. All samples except the supercritical sample exhibit a doublet at approximately 1,550 cm^{-1} and approximately 1,600 cm^{-1}, whereas the supercritical sample has a single peak at 1,585 cm^{-1} in this frequency range. The

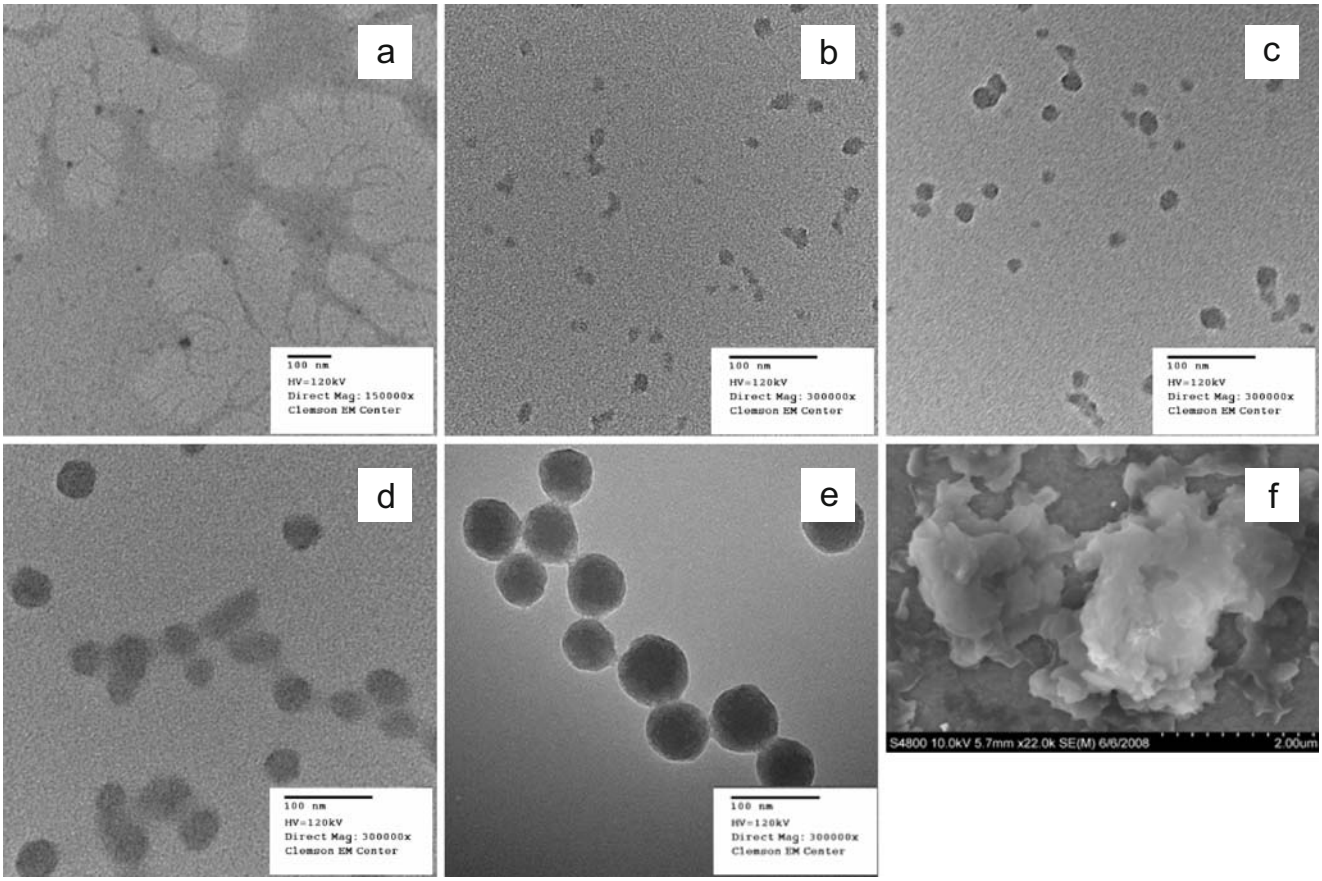

Fig. 1 C NPs and aggregates: **a** Fructose concentration, 0.3 M; reaction time, 7 h; reaction temperature, 110 °C; **b** 0.2 M, 12 h, 110 °C; **c** 0.3 M, 12 h, 110 °C; **d** 0.5 M, 12 h, 110°C; **e** 0.4 M, 7 h, 130 °C; **f** Conc. C NPs, 1 week, 400 °C

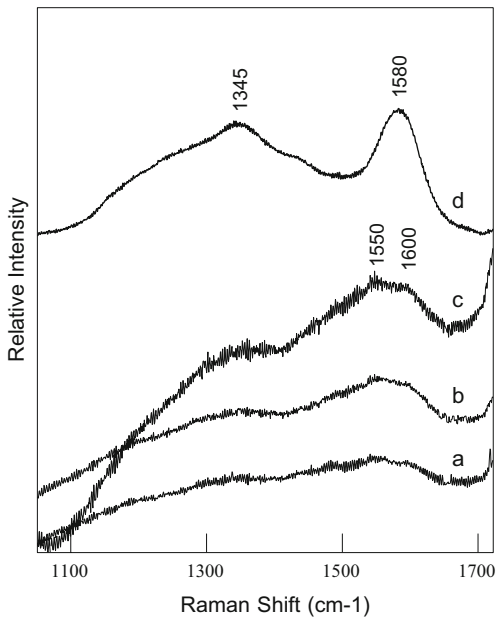

Fig. 2 Raman spectra of C NPs: **a** 0.3 M fructose heated for 7 h at 110 °C; **b** 0.3 M, 12 h, 110 °C; **c** 0.4 M, 7 h, 130 °C; **d** Conc. C NPs, 1 week, 400 °C

overall Raman spectra are characteristic of disordered carbon containing microcrystalline graphite phase that increased in samples treated with higher temperature and longer reaction time. The G-band is already present, albeit weak, in the sample treated for 7 h at 110°C (Fig. 2a), and its intensity increased after extending the reaction time to 12 h at the same temperature (Fig. 2b) or carrying out the reaction at 130 °C for 7 h (Fig. 2c). After the supercritical treatment, however, the G-band characteristic of microcrystalline graphite substantially intensified and sharpened (Fig. 2d). It was found that graphite formation from the hydrothermal reaction of fructose did not depend on the presence of silver but only on the temperature and duration of the reaction.

The hydrothermal reaction of fructose was also performed in the presence of Ag NPs resulting in the formation of carbon shells around the NPs. The first stage of the shell growth involved self-assembly of fructose dehydration product molecules on the Ag NP surface. These carbonyl-functionalized molecules adsorbed on the Ag NP surface by ion-dipole attraction and hydrogen bonding to Ag^{+} and $Ag(OH)_2^{-}$ species and formed large seeds for further growth of the carbon shells, which proceeded as explained above for

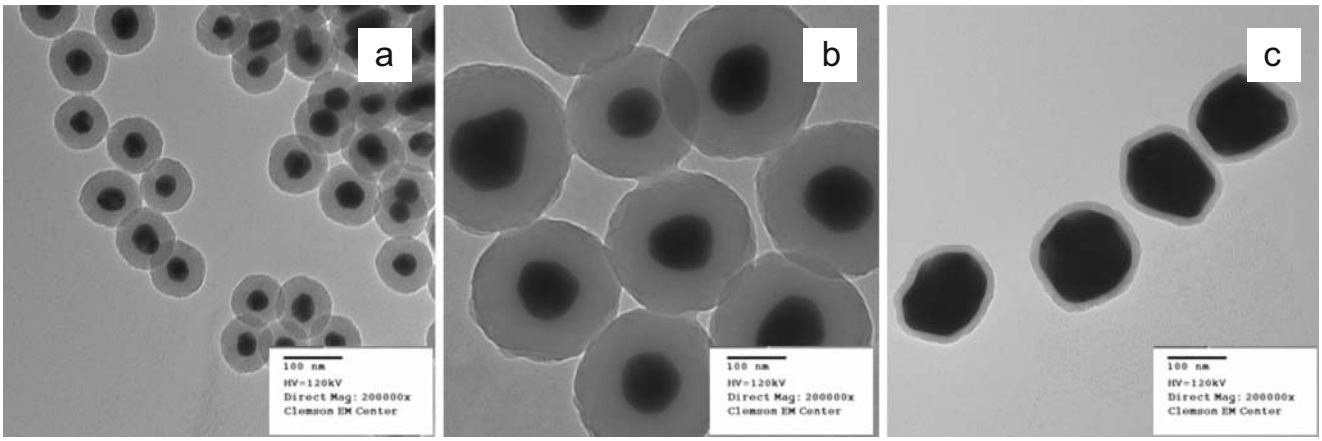

Fig. 3 Images of various C:Ag NPs: **a** 50 nm Ag NPs synthesized with 0.3 M fructose; **b** 100 nm Ag NPs, 0.4 M fructose; **c** 150 nm Ag NPs, 0.2 M fructose

C NPs. Carbon shells of varying thickness were formed around Ag NPs with varying diameters, three of which, 50, 100, and 150 nm, are discussed here (Fig. 3). The fructose concentration ranged from 0.1 to 0.4 M corresponding to carbon shells from 7 to 75 nm thick. Carbon shell thickness increased nonlinearly with increasing fructose concentration. C:Ag NPs with shells less than 10 nm thick, obtained from the reaction with 0.1 M fructose, had the tendency to aggregate during the reaction and were not reproducible for all NP sizes.

One of the purposes for carbon shells is for the protection of Ag NPs while maintaining their optical properties. Carbon has a large imaginary part of the dielectric function that causes light absorption in the visible spectral range; therefore, carbon shells can cause damping of the plasmon resonances of Ag NPs. It was reasoned that an optimum shell thickness can be determined that will provide protection for the Ag NPs with minimum damping of the plasmon resonance. The carbon shell had a strong effect on the plasmon resonance of Ag NPs by shifting it into the red spectral region as the shell thickness was increased (Fig. 4). For the 50 nm Ag NPs, a 70-nm red shift was observed after the reaction with 0.2 M fructose, and a further increase of fructose concentration did not result in more red shift even though thicker shells were produced. For 100 and 150 nm Ag NPs, the plasmon resonance continued shifting to the red with increase of the shell thickness. This behavior can be rationalized by considering how far the local electromagnetic field associated with the oscillating electrons extends from the surface of the Ag NP [11]. The field extends further from larger particles as compared to smaller ones. The red shifts of the plasmon

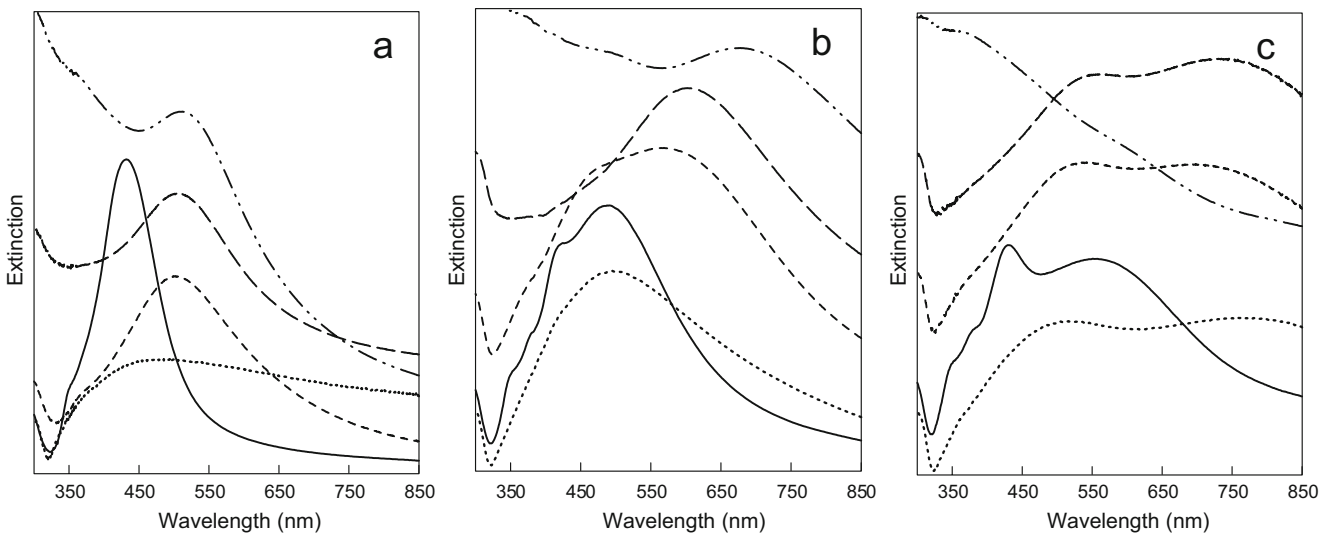

Fig. 4 UV–vis extinction spectra of C:Ag NP synthesized with **a** 50 nm Ag NPs, **b** 100 nm Ag NPs, and **c** 150 nm Ag NPs. *Solid lines* correspond to unmodified Ag NP, *dotted lines* correspond to C:Ag NPs synthesized with 0.1 M fructose, *short dashed lines*—0.2 M fructose, *long dashed lines*—0.3 M fructose, and *dash-dot-dot lines*—0.4 M fructose

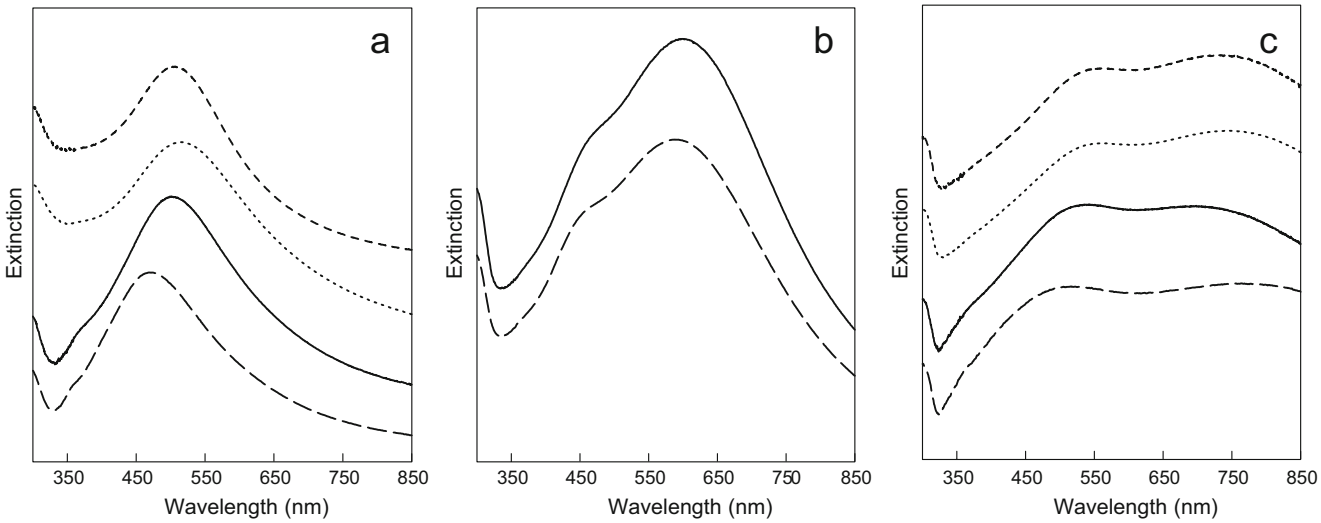

Fig. 5 UV–vis extinction spectra of C:Ag NP synthesized with **a** 50 nm Ag NPs, **b** 100 nm Ag NPs, and **c** 150 nm Ag NPs. Before (*solid lines*) and after (*long dashed lines*) the exposure to 0.2 M NaCl for 24 h refer to C:Ag NPs synthesized with 0.2 M fructose in **a** and **c** and 0.25 M in fructose in **b**. Before (*short dashed lines*) and after (*dotted lines*) NaCl exposure refer to C:Ag NPs synthesized with 0.3 M fructose in **a** and **c**. Spectra are offset for better visibility

resonance in C:Ag NPs originated from the increase of the local dielectric function due to the deposition of the carbon shells. The thicker the shell, the larger the local dielectric function and the more shift is produced. However, this process stops after the thickness of the shell exceeds the maximum distance to which the local field extends [11]. For smaller Ag NPs, the maximum distance is shorter, so the red shift of the plasmon resonance stopped with thinner carbon shells (Fig. 4a), whereas the red shift continued with the increase of the carbon shell thickness for larger Ag NPs. In addition to the red shift, the carbon shells produced damping of the plasmon resonance, as was evident from the decrease of the resonance intensity as well as a gradual increase of the extinction further in the blue spectral range. Extreme plasmon damping can be observed for 150 nm Ag NPs with the thickest carbon shell (75 nm) for which the plasmon resonance peak completely disappeared (Fig. 4c, dash-dot-dot line). The thicker the shell, the larger the contribution from the imaginary part of the dielectric function, resulting in more plasmon damping. The gradual increase of the background extinction as the shells grew was due to the absorbance and scattering from the carbon.

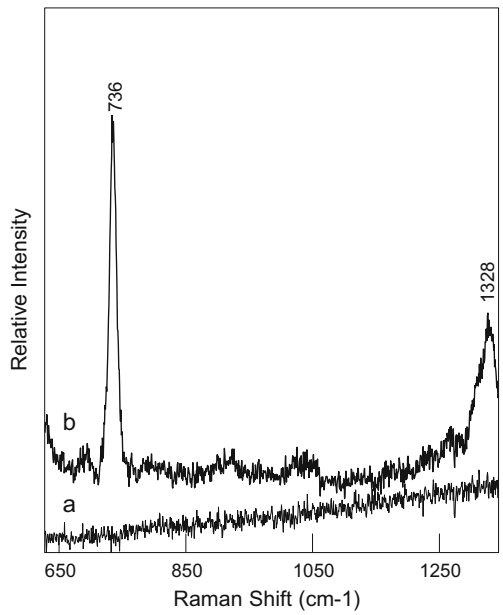

Fig. 6 SERS spectra of **a** C:Ag NPs and **b** uncoated Ag NPs after exposure to adenine

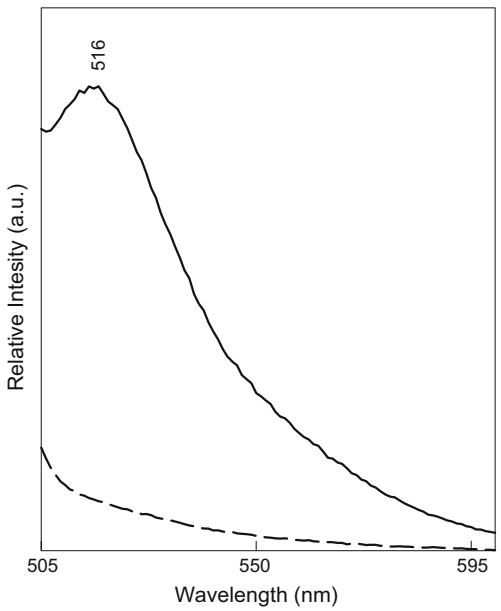

Fig. 7 C:Ag NP reaction with Alexa Fluor 488. *Solid line*: with carbohydrazide. *Dashed line*: no carbohydrazide

Stability of the C:Ag NPs was studied by exposing the NPs to 0.2 M sodium chloride solution. The addition of NaCl to uncoated Ag NPs initiated immediate aggregation, and the suspension became clear after a couple hours. On the contrary, C:Ag NPs remained stable after 24 h exposure to the chloride solution (Fig. 5). Even though C:Ag NPs with thin shells were stabilized against aggregation, the exposure to the chloride solution caused a blue shift of the plasmon resonance (long dashed lines in Fig. 5a,c). The blue shift was due to the chemisorption of chloride ions on the silver surface which donated electron density to the Ag NPs [34]. Chloride ions had less of an effect on the plasmon resonance of C:Ag NPs with thicker carbon shells. These results suggest that the carbon shells were porous. Small pores (0.4 nm) were previously reported in large carbon spheres synthesized from the hydrothermal reaction of glucose in water [19]. A SERS experiment was undertaken in order to estimate the pore size in C:Ag NPs. Uncoated 100 nm Ag NPs and the same NPs with carbon shells synthesized from 0.25 M fructose were exposed to an adenine-saturated solution for period of 4 h, and SERS spectra were measured. Whereas uncoated NPs exhibited a characteristic SERS spectrum of adenine, C:Ag NPs did not yield any SERS spectra under the same experimental conditions (Fig. 6). This result indicates that the adenine molecules did not reach the silver surface and the pore size in the carbon shells is smaller than adenine molecules (estimated 0.5 nm [35]). The combined results of the above experiments suggest that as the carbon shell became thicker, the porosity decreased due to increasing layers of carbon, so that thicker shells completely protected Ag NPs from the surrounding environment.

In order to explore the potential for the surface modification of C:Ag NP, a hydrazine–carbonyl cross-linking reaction was performed. This reaction is well known and is often used for quantifying sugars and levels of protein oxidation [36, 37]. The carbonyl-functionalized fluorescent dye Alexa Fluor 488 was linked to carbonyl groups on the surface of the C:Ag NPs by the symmetric cross-linker carbohydrazide. Spectra from the reaction can be seen in Fig. 7. The reported emission maximum of Alexa Fluor 488 is 519 nm, and the measured fluorescence from the dye-modified C:Ag NPs was 3 nm blue-shifted, indicating that the dye was attached to the carbon surface via carbohydrazide (Fig. 7, solid line). Carbohydrazide itself is a non-fluorescent molecule, and controlled experiments revealed no indication that Alexa Fluor 488 reacted with or adsorbed onto/into the carbon shell when no carbohydrazide was present (Fig. 7, dashed line). Quantification of the dye linked to the surface of C:Ag NPs from the fluorescence data was difficult due to potential fluorescence quenching by the carbon shell.

Conclusion

The hydrothermal reaction of fructose allows the synthesis of carbon NPs starting from 10 nm to at least 1 μm in diameter. Their size, rate of growth, and the degree of carbonization can be controlled by changing fructose concentration, reaction time, and temperature. The reaction can be used for synthesis of carbon shells around NPs as was exemplified using Ag NPs of various sizes. The same parameters that control the size of carbon NPs also control the thickness of the shells. The shell thickness around Ag NPs can be adjusted to provide protection and stabilization for the NPs in high salt concentrations, at the same time to have a minimum damping effect on the plasmon resonance. The carbon shell offers a scaffold for surface modifications via carbohydrazide coupling to the surface carbonyl groups. Strong plasmon resonance, stability at physiological salt concentrations, and the possibility for attaching proteins or other molecules using standard cross-linking methods make C:Ag NP a promising system for biological applications, for example for optical labeling and imaging.

Acknowledgments The authors thank the Department of Energy, grant no. DE-FG02-06ER46342 for funding this research, the Clemson University Electron Microscopy Facility, and Dr. Kenneth A. Christensen and his research group for some of the equipment used in this work. We also thank Dr. Joseph W. Kolis and Matthew Mann for providing help and equipment for the supercritical treatment of C NPs.

References

1. Kreibig U, Vollmer M (1995) Optical properties of metal clusters; Springer Series in Materials Science 25. Springer, New York
2. Evanoff DD Jr, Chumanov G (2005) ChemPhysChem 6:1221–1231
3. Daniels JK, Caldwell TP, Christensen KA, Chumanov G (2006) Anal Chem 78:1724–1729
4. Kinnan MK, Chumanov G (2007) J Phys Chem C 111:18010–18017
5. Lukomska J, Malicka J, Gryczynski I, Lakowicz JR (2004) J Fluor 14:417–423
6. Aslan K, Wu M, Lakowicz JR, Geddes CD (2007) J Am Chem Soc 129:1524–1525
7. Lee S, Kim S, Choo J, Shin SY, Lee YH, Choi HY, Ha S, Kang K, Oh CH (2007) Anal Chem 79:916–922
8. Tai S-P, Wu Y, Shieh D-B, Chen L-J, Lin K-J, Yu C-H, Chu S-W, Chang C-H, Shi X-Y, Wen Y-C, Lin K-H, Liu T-M, Sun C-K (2007) Adv Mater 19:4520–4523
9. Huang T, Nallathamby PD, Gillet D, Xu XN (2007) Anal Chem 79:7708–7718
10. Hu Q, Tay L-L, Noestheden M, Pezacki JP (2007) J Am Chem Soc 129:14–15
11. Evanoff DD Jr, White RL, Chumanov G (2004) J Phys Chem B 108:1522–1524
12. Kumbhar A, Chumanov G (2004) J Nanosci Nanotech 4:299–303
13. Quaroni L, Chumanov G (1999) J Am Chem Soc 121:10642–10643

14. Perez-Mendez M, Marsal-Berenguel R, Sanchez-Cortes S (2004) App Spec 58:562–569
15. Li T, Park HG, Lee HS, Choi SH (2004) Nanotech 15:S660–S663
16. Logothetidis S (2007) Diamond Related Mat 16:1847–1857
17. Yao C, Shin Y, Wang L, Windisch CF Jr, Samuels WD, Arey BW, Wang C, Risen WM Jr, Exarhos GJ (2007) J Phys Chem C 111:15141–15145
18. Sun X, Li Y (2004) Angew Chem Int Ed 43:597–601
19. Wang Q, Li H, Chen L, Huang X (2001) Carbon 39:2211–2214
20. Titirici MM, Thomas A, Yu S-H, Muller J-O, Antonietti M (2007) Chem Mater 19:4205–4212
21. Wang Z, Xiao P, He N (2006) Carbon 44:3277–3284
22. Caiulo N, Yu CH, Yu KMK, Lo CCH, Oduro W, Thiebaut B, Bishop P, Tsang SC (2007) Adv Funct Mater 17:1392–1396
23. Yu S-H, Cui X, Li L, Li K, Yu B, Antonietti M, Colfen H (2004) Adv Mater 16:1636–1640
24. Sun X, Li Y (2005) Langmuir 21:6019–6024
25. Yu JC, Hu X, Li Q, Zhang L (2005) Chem Commun 21:2704–2706
26. Fang Z, Tang K, Lei S, Li T (2006) Nanotechnology 17:3008–3011
27. Luo LB, Yu SH, Qian HS, Gong JY (2006) Chem Commun 7:793–795
28. Evanoff DD Jr, Chumanov G (2004) J Phys Chem B 108:13948–13956
29. Kuster BFM, Terbens LM (1976) Carbohydr Res 54:159–164
30. Kuster BFM, van der Baan HS (1976) Carbohydr Res 54:165–176
31. Kuster BFM, Temmink HMG (1976) Carbohydr Res 54:185–191
32. Antal MJ, Mok WS (1990) Carbohydr Res 199:91–109
33. Schwan J, Ulrich S, Batori V, Ehrhardt H, Silva SRP (1996) J Appl Phys 80:440–447
34. Henglein A (1993) J Phys Chem 97:679–682
35. Takenaka A, Shibata M, Sasada Y (1986) Acta Crystallogr C42:1336–1340
36. Fields R, Dixon HBF (1971) Biochem J 121:587–589
37. Ahn B, Rhee SG, Stadtman ER (1987) Anal Biochem 161:245–257